Faraday Discussions

Cite this: *Faraday Discuss.*, 2015, **182**, 227

PAPER

Oxygen deficient layered double perovskite as an active cathode for CO_2 electrolysis using a solid oxide conductor

Tae Ho Shin,*[ac] Jae-Ha Myung,[a] Maarten Verbraeken,[a] Guntae Kim[b] and John T. S. Irvine*[a]

Received 17th February 2015, Accepted 26th March 2015
DOI: 10.1039/c5fd00025d

A-site ordered $PrBaMn_2O_{5+\delta}$ was investigated as a potential cathode for CO_2 electrolysis using a $La_{0.9}Sr_{0.1}Ga_{0.8}Mg_{0.2}O_3$ (LSGM) electrolyte. The A-site ordered layered double perovskite, $PrBaMn_2O_{5+\delta}$, was found to enhance electrocatalytic activity for CO_2 reduction on the cathode side since it supports mixed valent transition metal cations such as Mn, which could provide high electrical conductivity and maintain a large oxygen vacancy content, contributing to fast oxygen ion diffusion. It was found that during the oxidation of the reduced $PrBaMn_2O_{5+\delta}$ (O5 phase) to $PrBaMn_2O_{6-\delta}$ (O6 phase), a reversible oxygen switchover in the lattice takes place. In addition, here the successful CO_2 electrolysis was measured in LSGM electrolyte with this novel oxide electrode. It was found that this $PrBaMn_2O_{5+\delta}$, layered perovskite cathode exhibits a performance with a current density of 0.85 A cm^{-2} at 1.5 V and 850 °C and the electrochemical properties were also evaluated by impedance spectroscopy.

1. Introduction

With growth of renewable energy technologies, it is necessary to store vast amounts of energy by, *e.g.*, converting electricity overcapacity to chemical energy in the form of compounds such as hydrogen, methane, or methanol. In particular, the variety of products from high temperature electrolysis can be used as feedstocks for chemical synthesis or converted into highly dense electric power; it would provide a means of storing renewable electricity in a convenient, high energy-density form. Recently, hydrogen has attracted attention as an alternative mediator for energy conversion and storage because of its high gravimetric energy density and zero carbon emission.[1–5] However, the utilization of hydrogen has been limited due to the practical engineering and economic limitations with

[a]*School of Chemistry, University of St Andrews, St Andrews, Fife, KY16 9ST, Scotland, UK. E-mail: ths@st-andrews.ac.uk; ceramist95@gmail.com; Tel: +44-(0)759-676-2424*
[b]*Dept. of Chemical and Energy Engineering, Ulsan National Institute of Science and Technology (UNIST), Korea*
[c]*Electronic Materials Convergence Division, Korea Institute of Ceramic Engineering & Technology (KICET), Korea*

respect to its generation and distribution.[6] On the other hand hydrocarbon fuels and carbon monoxide cost-effectively match the existing energy infrastructure well because of their similarity to current fossil fuels; they would be effective energy carriers in a period of transition toward zero carbon emission.[7–9] Recycling or reuse of CO_2 could be an effective approach for accessing a new form of energy carrier and enabling a carbon-neutral cycle. In particular, electrochemical reduction of CO_2 into CO fuel with renewable electricity has been proposed as an alternative method to store this energy, overcoming the inherent problems with intermittency and geographical distribution of renewable energy sources.[10–13]

Solid oxide electrolysis cells (SOECs) have recently attracted a great deal of interest as a highly efficient electrolyser and a green energy technology. Current developments are mainly based upon steam electrolysis for hydrogen production. However, reduction of CO_2 using a highly efficient solid oxide electrolyser is also feasible. This would be an alternative to carbon capture and advanced utilization of CO_2.[14,15] Solid oxide electrolysers with oxygen ion conducting electrolytes are able to separately produce CO and O_2 from CO_2 ($CO_2 \rightarrow 1/2O_2 + CO$) at high and intermediate temperature (500–900 °C) with high efficiencies (as they are not limited by the Carnot cycle). Both products, CO and O_2 may be useful in industrial processes. The electrolysis of CO_2 in a solid oxide device is analogous to high temperature steam electrolysis by SOECs, *i.e.* CO_2 molecules are electrochemically reduced into CO at the cathode (fuel electrode) and oxygen ions are transported through the oxygen-ion conducting electrolyte to the anode (oxygen electrode) where gaseous O_2 is produced and released. High temperature solid oxide electrolysis reduces electricity demand, and offers fast electrode kinetics, reducing the overall cell internal resistance as a consequence and increasing electrolysis efficiency. Due to the operating conditions in SOECs using CO_2, cathode materials require stability in a wide pO_2 and temperature range, and additionally need to be tolerant towards carbon coking. To date, SOECs predominantly comprise materials and techniques from solid oxide fuel cells (SOFCs), but operated in reverse modes. This means that electrode materials have not been tailored specifically for use in electrolysis conditions, which can differ substantially from fuel cell conditions. Long term stability of solid oxide electrode materials is still one of the important challenging issues for both SOECs and SOFCs for commercialisation into the energy market.

Currently, high temperature electrolysis of CO_2 has been mainly performed using Ni–YSZ cermet cathodes in oxygen ion conducting SOECs. However, Ni is easily deactivated by reoxidation or carbon formation when it is directly exposed to CO/CO_2 or a hydrocarbon atmosphere.[16–18] Therefore, a significant reduction atmosphere is required to flow over the Ni surface base electrode to avoid oxidation of Ni to NiO, which would cause a loss of electronic conductivity and the failure of the electrode. In the most serious circumstances, the electrode fails mechanically as a result of deposited coke or re-oxidation.[19] Consequently, redox stability and reversibility have recently been emphasised as important requirements for the cathode (fuel electrode) material in SOECs. So far, several conductive perovskite oxides have been reported as potential anode materials in SOFCs, which may also be useful as cathode materials in SOECs. For more sturdy and superior materials in durable SOFC/SOEC systems, various mixed ionic and electronic conducting (MIEC) oxides have been explored. Among these, researchers have mainly demonstrated that $La(Sr)MO_3$ (M = Cr, Mn, Fe, Ti)

perovskite oxides[20–22] can, in principle, be good fuel electrode materials with sufficient electronic conductivity. For instance, the efficient electrolysis of CO_2 based on a ceramic cathode, La(Sr)Mn(Cr)O_3 (LSCM) perovskite oxide have been recently demonstrated.[20,23–25] However, electrochemical performance of the ceramic electrodes is still smaller than that using a Ni based electrode, due to insufficient electrical conductivity and low electrocatalytic activity. LSCM suffers from a drop in conductivity under the reducing SOEC cathode conditions.

Recently we have succeeded in synthesising the oxygen deficient layered phase, $PrBaMn_2O_{5+\delta}$ under reducing atmosphere. Whereas polycrystalline samples sintered in air adopt the cubic ABO_3 perovskite structure, the A-site ordered layered perovskite $PrBaMn_2O_{5+\delta}$, can be grown under reducing conditions. Furthermore, it was found that the double perovskite, $PrBaMn_2O_{5+\delta}$ exhibits high electrical conductivity and excellent redox and coking tolerance when used as an anode for an SOFC.[26] In this work, $PrBaMn_2O_{5+\delta}$, employed as a potential ceramic cathode for CO_2 electrolysis SOEC with a configuration of $PrBaMn_2O_{5+\delta}$|La doped ceria (LDC)|$La_{0.9}Sr_{0.1}Ga_{0.8}Mg_{0.2}O_3$ (LSGM)|La(Sr)Fe(Co)O_3. The performance of the $PrBaMn_2O_{5+\delta}$ cathode and the electrochemical process of high temperature electrolysis of CO_2 in a cell using LSGM as the electrolyte were investigated and evaluated.

2. Experimental

The $Pr_{0.5}Ba_{0.5}MnO_{3-\delta}$ was prepared using the conventional solid-state reaction method and then A-site ordered layered $PrBaMn_2O_{5+\delta}$ is obtained by *in situ* annealing of $Pr_{0.5}Ba_{0.5}MnO_{3-\delta}$ in reducing conditions using 5% H_2 at temperatures higher than 800 °C. The crystalline phase characterization of the oxide powder was performed by X-ray diffraction (PANalytical Empyrean, Mo Kα radiation and Cu Kα1 radiation). Thermal gravimetric analysis (TGA) was carried out on a NETZSCH TG 209 instrument (NETZSCH Geraetebau GmbH, Selb, Germany) with a heating & cooling rate of 2–5 °C min^{-1} to evaluate the oxygen loss and incorporation on redox cycling in air and 5% H_2 on the compositions synthesized and dilatometry was also performed at 100 °C to 800 °C with a heating/cooling rate of 2 °C min^{-1} in air and 5% H_2 to characterize the thermo-physical properties. Electrical conductivity was measured on the sintered pellets by the standard four terminal DC method or van der Pauw method up to 900 °C in ambient air. A current of 50 mA (model: Keithley 220, Keithley Instruments Inc., U.S.A.) was applied in both directions, and resistance was calculated as a gradient of potential *vs.* current. These conductivity details were previously reported.[26]

For solid oxide electrolyser experiments, a configuration of $PrBaMn_2O_{5+\delta}$|LDC|$La_{0.9}Sr_{0.1}Ga_{0.8}Mg_{0.2}O_3$ (LSGM)|La(Sr)Fe(Co)O_3 was fabricated using 200 μm thick LSGM electrolyte supports. Commercially available powder, $La_{0.9}Sr_{0.1}Ga_{0.8}Mg_{0.2}O_{3-\delta}$ (LSGM, 99.9% Kceracell co., Ltd, South Korea) was used for the preparation of electrolyte. The LSGM electrolyte supports were prepared by dry-pressing powder into a circular green body followed by high-temperature sintering in air at 1450 °C for 6 h and mechanical polishing until 2 cm diameter and 200 μm thick electrolyte supports were obtained. Electrodes were deposited onto the faces of the LSGM electrolyte disk by screen-printing inks of the respective powders, followed by sintering at 1100 °C for 30 min (thickness of screen printed electrode, <25 μm). The active area of the cells, equal to the area to the cathode area ($PrBaMn_2O_{5+\delta}$), was 0.5 cm^2 and the area of the anode was same.

To evaluate the electrochemical properties, *I–V* curves and impedance were measured using a four terminal configuration with silver mesh/wire as the electrode current collectors. In order to perform electrochemical testing in fuel cell mode, a dried CO_2/CO (70 : 30 vol) mixture was supplied into the cathode with a 100 ml min^{-1} flow rate while the anode side was exposed to constant oxygen flow as an oxidant gas (100 ml min^{-1}). The cell was maintained in each condition for at least one hour to reach steady state, before carrying out any electrochemical tests. AC impedance spectroscopy was recorded using an IM6 Electrochemical Workstation (Zahner, Germany) with frequency ranged from 0.1 Hz to 100 kHz with an amplitude of 10 mV.

3. Results and discussion

The disordered cubic perovskite $Pr_{0.5}Ba_{0.5}MnO_3$ was prepared by a typical solid state reaction. To avoid the complete oxidization of Mn^{3+} to Mn^{4+}, which would favour the formation of $BaMnO_3$, the powder was calcined in an atmosphere with lower oxygen partial pressure (using a mixture of Ar/air) below the synthesis temperature (<1300 °C). A-site ordering in the layered manganite perovskite would be partially hindered by the formation of the hexagonal related perovskite $BaMnO_3$. Fig. 1 shows the XRD pattern for the cubic disordered perovskite (Fig. 1a), prepared by solid state reaction at 1200 °C in air; reduction in 5% H_2 leads to A-site ordering and hence doubling of the unit cell, giving a layered phase with tetragonal symmetry (Fig. 1b). The XRD pattern of disordered cubic perovskite shown in Fig. 1a, suggests the presence of a small amount secondary hexagonal phase, as similarly observed in a previous study in which the powder was prepared by Pechini synthesis at lower temperature.[26] However, they are not serious impurities but a single phase of $Pr_{0.5}Ba_{0.5}MnO_3$ was mainly indicated. Furthermore, the A-site ordered layered perovskite $PrBaMn_2O_{5+\delta}$ could also be grown by annealing the disordered phase in reducing atmosphere in accordance

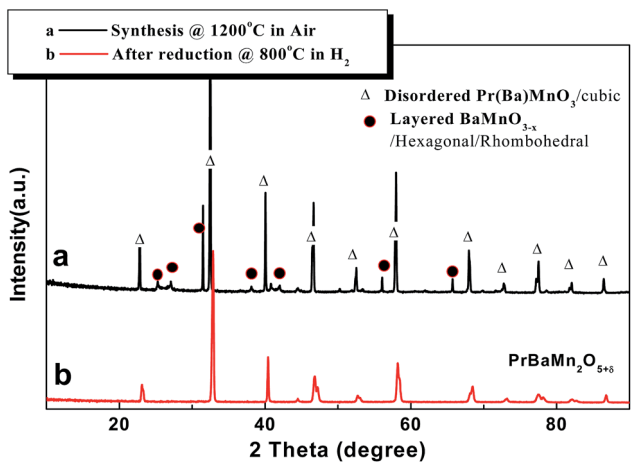

Fig. 1 X-ray diffraction patterns of (a) $Pr_{0.5}Ba_{0.5}MnO_3$ (O3) prepared by solid state reaction at 1200 °C in air, and (b) $PrBaMn_2O_{5+\delta}$ (O5) was obtained by reducing the as-prepared powder in 5% H_2 at 800 °C for 4 h (Cu Kα radiation).

with previous results.[26] To fully understand the phase changes during redox cycling, we checked the phase transition from disordered cubic $Pr_{0.5}Ba_{0.5}MnO_3$ phase (O3) to oxygen deficient layered $PrBaMn_2O_{5+\delta}$ (O5) by *in situ* variable temperature/atmosphere X-ray diffraction (Mo Kα1/Kα2), whilst performing reduction–oxidation cycles. Fig. 2a–c shows Rietveld refinement profiles of $Pr_{0.5}Ba_{0.5}MnO_3$ phase (O3), $PrBaMn_2O_{5+\delta}$ (O5) and $PrBaMn_2O_{6-\delta}$ (O6) from *in situ* XRD data at 800 °C in various atmospheres. The refined unit cell parameters and refinement statistics are summarized in Tables 1 and 2 and show selected bond distances and angles.

The *in situ* high temperature X-ray diffraction study confirms cubic symmetry for the disordered O3 phase at 800 °C. Upon reduction at 800 °C, the A-site ordered O5 phase emerges with tetragonal symmetry, causing a relative shrinkage of the *c*-axis as compared to the *a*-axis. Refinement is successful using the *P*4/*mmm* space group. Subsequent re-oxidation of the A-site ordered O5 phase at 800 °C results in the emergence of the double perovskite, $PrBaMn_2O_{6-\delta}$ (O6) phase. This O6 phase also has tetragonal symmetry with space group *P*4/*mmm*. Re-oxidation of the O5 phase causes a decrease in tetragonality as evidenced by the drop in $2a/c$ ratio from 1.018 to 1.005. Despite this, direct evidence of A-site ordering and thus doubling of unit cell in both O5 and O6 phased from the XRD data is the (001) reflection found at $2\theta \approx 5°$as shown in Fig. 2b and c. Despite the weak intensity of the (001) reflection due to small contrast between Pr^{3+} and Ba^{2+}, its emergence on redox cycling is significant.

The fully oxidised ordered O6 phase shows A-site ordering along the *c*-axis, with a stacking pattern of alternating BaO–MnO_2–PrO–MnO_2–BaO layers. As expected from perovskite materials, Mn is six coordinated, whereas both Ba and Pr are twelve coordinated. The MnO_6 octahedron is slightly distorted, causing the Mn and O2 sites to be closer to Pr than to Ba. The reduced O5 variant has an identical stacking sequence but additionally exhibits oxygen vacancy ordering, with the O3 site vacant, resulting in Pr layers without oxygen ions, shown in Fig. 3. In this structure Mn becomes square pyramidally coordinated, whereas Pr is now 8 coordinated to O2. Ba becomes less coordinated to O2, as the latter moves closer to Pr. The lattice volume is increased due to Mn reduction as shown in Tables 1 and 2.

Due to the reduction of Mn^{3+}/Mn^{4+} in the O3/O6 phases to Mn^{2+}/Mn^{3+} in O5 the Mn–O bond length at 800 °C increases from 1.89–2.03 to 2.04–2.07 Å. It is expected that the oxygen deficient PrO_x layer provides a channel for fast oxygen transport and therefore A-site ordering is in fact enhancing the oxygen mobility, albeit only in two dimensions.[27] The coexistence of Mn oxidation states is further expected to give rise to electronic conductivity, which is a requirement for any SOEC/SOFC electrode material. The mixed valence of transition metals such as Mn could give rise to different Mn–O bond lengths at various oxygen partial pressure conditions; the swollen Mn–O bonding length (*ca.* 2.046 Å) of the oxygen deficient phase could be expected from the reduced oxidation state of Mn (Mn^{3+} or Mn^{2+}). The vacancy would be mainly located between reduced Mn^{3+}/Mn^{2+} state cations, between pairs of square pyramidal MnO_5. Thus oxygen vacancy ordering provides a mechanism to reduce the coordination number of the smaller Pr^{3+} ion without reducing the coordination number of the larger Ba^{2+} ion. Under reducing conditions, oxygen atoms in the PrO_x plane can be partially or entirely removed,

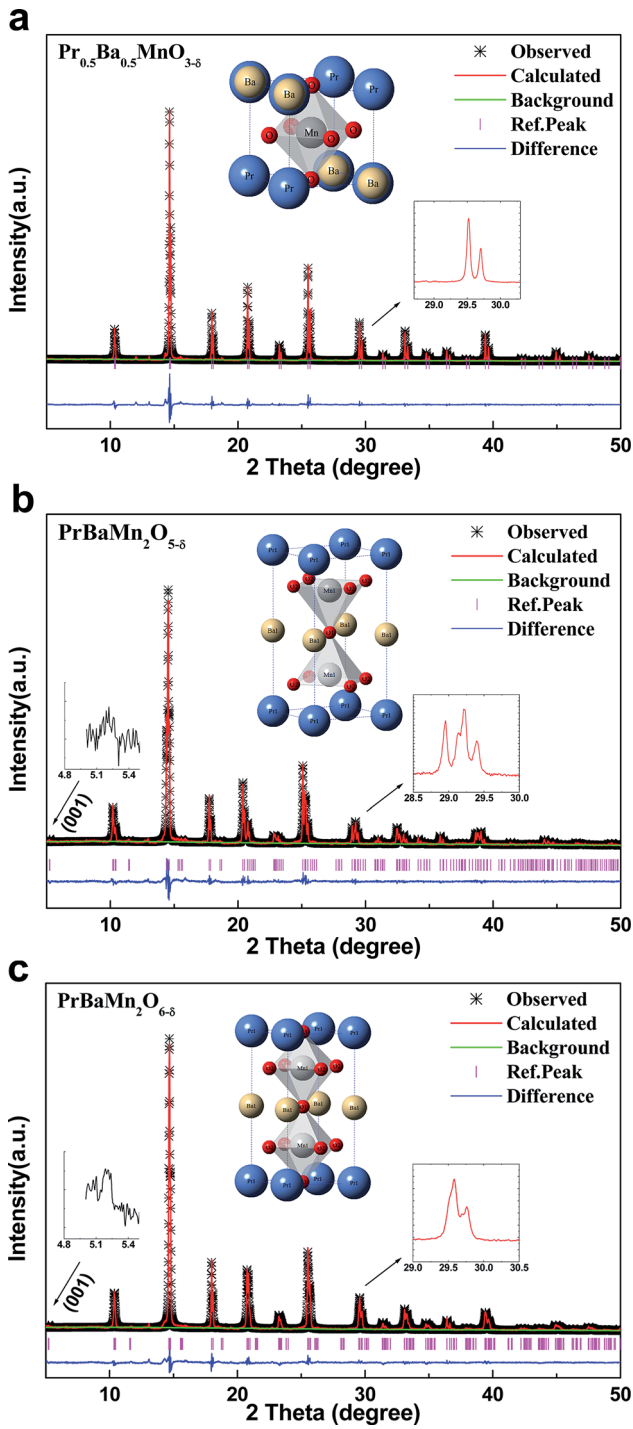

Fig. 2 Rietveld-refined XRD profiles of (a) $Pr_{0.5}Ba_{0.5}MnO_3$ (O3), (b) $PrBaMn_2O_{5+\delta}$ (O5) and (c) $PrBaMn_2O_{6-\delta}$ (O6) obtained by simultaneous fitting of *in situ* high temperature XRD data at 800 °C in air, 5% H_2 and air, respectively. (Mo Kα1, Kα2 radiation).

Table 1 Refined structural parameters for $Pr_{0.5}Ba_{0.5}MnO_3$ (O3), $PrBaMn_2O_{5+\delta}$ (O5) and $PrBaMn_2O_{6-\delta}$ (O6) obtained by simultaneous fitting of *in situ* high temperature XRD data at 800 °C

	$Pr_{0.5}Ba_{0.5}MnO_3$ (O3) in air	$PrBaMn_2O_{5+\delta}$ (O5) in H_2	$PrBaMn_2O_{6-\delta}$ (O6) in air
Space group	$Pm\bar{3}m$ (cubic)	$P4/nmm$ (tetra)	$P4/mmm$ (tetra)
$a = b$ (Å)	3.93593(5)	4.02405(9)	3.93985(9)
c (Å)	—	7.90618(24)	7.84136(24)
$2a/c$		1.018	1.005
V (Å^3)	60.9735(13)	128.024(6)	121.717(5)
λ (Å) Mo Kα1	0.0793	0.7093	0.7093
λ (Å) Mo Kα2	0.7136	0.7136	0.7136
R_p%	7.93	6.43	6.06
R_{wp}%	11.19	8.30	8.01

creating many oxygen vacant sites in the crystal sites. This might illustrate the close coupling between A-site ordering and oxygen vacancy ordering.[27]

What makes the layered perovskite-manganese oxide $PrBaMn_2O_{5+\delta}$ a promising candidate for high oxygen mobility is its remarkable variability in oxygen content under redox conditions. It was generally found that for $ReBaMn_2O_{5+\delta}$ (Re = Pr, Nd, La, Gd) the oxidation of the reduced (O5) phase $PrBaMn_2O_{6-\delta}$ (O6), in the case of $ReBaMn_2O_{5+\delta}$, a reversible oxygen switchover in the lattice takes place. The reversibility of the phase change during redox cycle was also established by thermal analysis. The fully oxygen charged $PrBaMn_2O_{6-\delta}$ (O6) had been reduced in 5% H_2/95% Ar at elevated temperature up to 800 °C and cooled in 5% H_2/95% Ar to room temperature (2.5 °C min^{-1}) and re-oxidized up to 700 °C in air. Fig. 4 shows the thermogravimetric analysis (TGA) in which a weight gain of *ca.* 3.58 wt % was observed on both reduction and re-oxidation corresponding to a loss/uptake of 1 formula unit of oxygen ($\delta = 1$). This symmetry between reduction and

Table 2 Selected interatomic distances and angles of $Pr_{0.5}Ba_{0.5}MnO_3$ (O3), $PrBaMn_2O_{5+\delta}$ (O5) and $PrBaMn_2O_{6-\delta}$ (O6) obtained by simultaneous fitting of *in situ* high temperature XRD data at 800 °C

	$Pr_{0.5}Ba_{0.5}MnO_3$ (O3) in air	$PrBaMn_2O_{5+\delta}$ (O5) in H_2	$PrBaMn_2O_{6-\delta}$ (O6) in air
Distance (Å)			
Mn–O1	1.96796(2) 6	2.067(5) × 1	2.03072(6) × 1
Mn–O2	—	2.0405(18) × 4	1.97022(4) × 4
Mn–O3	—	—	1.88996(6) × 1
Mn–O (average)	1.96796	2.0458	1.96693
Angles (°)			
Mn–O1–Mn	180	180	180
Mn–O2–Mn	—	160.83(57)	178.01680(10)
Mn–O3–Mn	—	—	180
O1–Mn–O3	180	—	180
O2–Mn–O2	180	160.83(57)	178.01680(10)

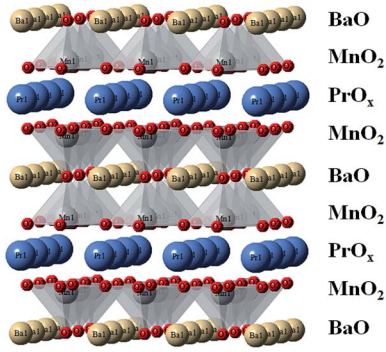

Fig. 3 A schematic drawing of crystal structure model determined for A-site ordering layered $PrBaMn_2O_{5+\delta}$ (O5) and oxygen vacancy ordering in oxygen deficient O5 phase by Rietveld-refined XRD profile.

oxidation cycles suggests excellent reversibility, which is in agreement with our previously reported dilatometry data.[26]

Since $PrBaMn_2O_{5+\delta}$ shows superior redox reversibility as well as potential electrochemical performance as oxide anode for SOFCs, application of $PrBaMn_2O_{5+\delta}$ for a potential cathode in CO_2 electrolysis using solid oxide ion conductor, LSGM, was further studied. Fig. 5a shows the temperature dependent *I–V* curves for CO_2 electrolysis between 750 °C and 850 °C under the following gas feed conditions: air on the anode side and a mixture of 70% CO_2/30% CO on the cathode side with 100 ml min^{-1}. It was found that $PrBaMn_2O_{5+\delta}$ is very effective for CO_2 electrolysis with a remarkable cathodic current density of 0.84 A cm^{-2} at 1.55 V and 850 °C. At lower temperature (750 °C), it seems that there was no significant current flow at lower voltages suggesting a slow electrolysis reaction, which might be explained by the large overpotential on the cathode side; the cell

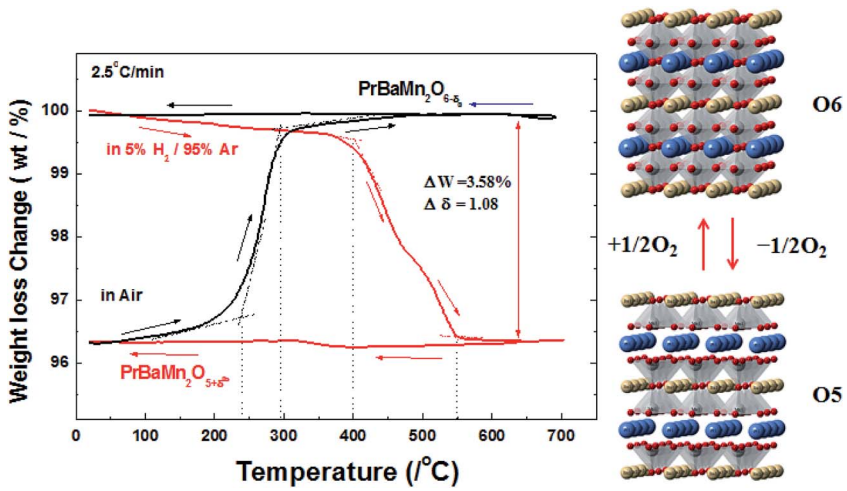

Fig. 4 TGA curves of $PrBaMn_2O_{5+\delta}$ in 5% H_2/Ar from room temperature to 700 °C to room temperature and in re-oxidation cycle from room temperature to 700 °C.

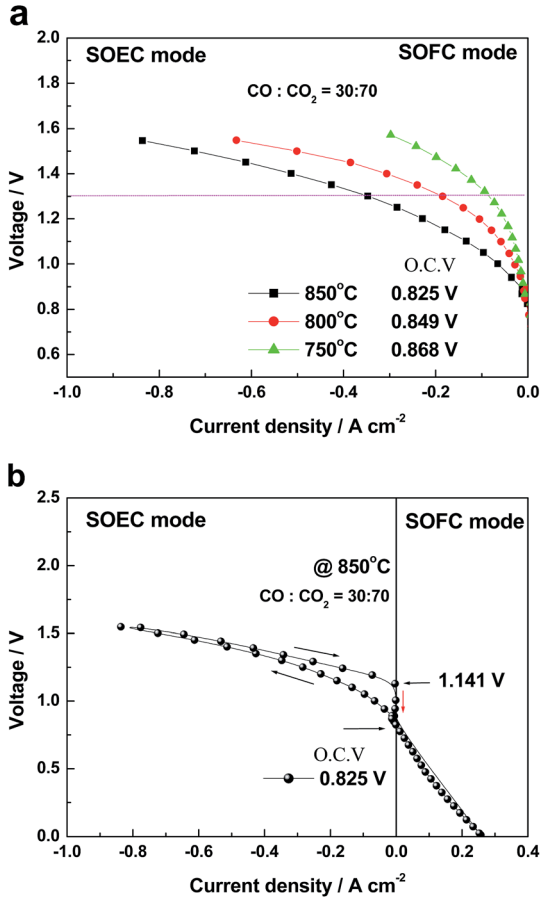

Fig. 5 (a) Temperature dependent *I–V* curves for CO_2 electrolysis under gas feed conditions with elevating temperature (750–850 °C) with the cell configuration of $PrBaMn_2O_{5+\delta}$|LDC|$La_{0.9}Sr_{0.1}Ga_{0.8}Mg_{0.2}O_3$ (LSGM)|La(Sr)Fe(Co)O_3 and (b) the *I–V* curves, voltages during steady current cycling at 850 °C.

voltage sharply increased with increasing current density at initial low current range. Fig. 5b shows the *I–V* curve at 850 °C, during current cycling, which was measured with increasing current up to the maximum current range and subsequent decreasing current, leaving long stabilisation times at every current step to attempt to attain equilibrium. However, it was observed that voltage recovery was slow and strongly time dependent. As shown in Fig. 5b, initial OCV (0.825 V) was slightly increased to 1.141 V after current cycling; the initial OCV was however recovered over time. The increased OCV after cycling could be related with momentary carbon deposition or carbon monoxide adsorption on the catalyst surface, as 1.14 V is very close to the theoretical OCV value for carbon fuel; slow surface kinetics of $PrBaMn_2O_{5+\delta}$ might explain such desorption/adsorption CO/CO_2 or carbon species. Alternatively, poor catalytic activity for carbon oxidation or a Ba carbonation reaction might play a role too. The slow chemical kinetics are not fully understood at this stage, but a more detailed analysis using *in situ*

exhausts gas analysis, catalyst additives and *in situ* surface analysis would be helpful to shed further light on the issue in future work. In particular, stable catalytic activity of $PrBaMn_2O_{5+\delta}$ for CO_2 could be improved with other catalyst additives, whereas B-site doping may help stabilize the Ba from carbonisation.

For the detailed reaction mechanisms, ac impedance spectra were measured. Fig. 6 shows complex impedance plots under open circuit conditions for internal resistance of the cell $PrBaMn_2O_{5+\delta}|LDC|La_{0.9}Sr_{0.1}Ga_{0.8}Mg_{0.2}O_3$ (LSGM)$|La(Sr)Fe(Co)O_3$. In general, it is necessary to have a reference electrode to separate anode and cathode losses. However, it should be recognized that improper placement of the reference electrode and working electrodes will give erroneous value; thus, exactly separating each electrode can be difficult even in a symmetric electrode geometry in a thin electrolyte support cell, when the kinetics of the two electrodes are significantly different.[28–30] As shown in Fig. 6a, it is significant that the ohmic resistance in both impedance spectra are approximately the same, and almost exactly one-half of the total ohmic resistance of the cell, showing that the reference electrode is sampling the

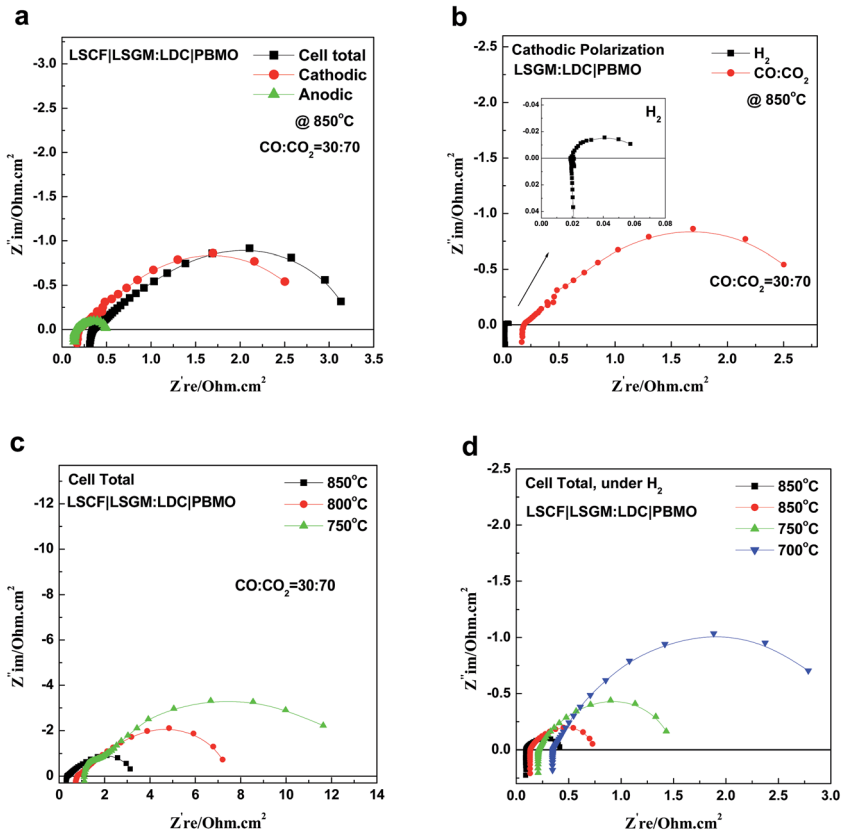

Fig. 6 Nyquist plot of the $PrBaMn_2O_{5+\delta}|LDC|La_{0.9}Sr_{0.1}Ga_{0.8}Mg_{0.2}O_3$ (LSGM)$|La(Sr)Fe(Co)O_3$ cell under open circuit: (a) impedance plot of cells, cathodic and anodic under 70% vol CO_2 gas fuel condition at 850 °C, (b) comparison of cathodic impedance plot under H_2 with 70% vol CO_2, (c) temperature dependant impedance plot of the total cell under 70% vol CO_2 gas fuel, (d) temperature dependant impedance plot of the total cell under H_2 gas fuel.

potential at the centre of the electrolyte. Thus, it can be roughly inferred that total polarization resistance was clearly dominated by cathodic electrode ($PrBaMn_2O_{5+\delta}$) because cathodic impedance spectra was similar to the total cell impedance. It is obvious that at least two semicircles are present in the impedance plot. Considering the response frequencies of the two parallel RQ circuits, the resistance at higher frequency (R_{p1}) could be assigned to a charge transfer process, whereas the lower frequency process (R_{p2}) seems related to a diffusion process of the cathodic reaction. The contribution of R_{p2} is much larger than that of the surface reaction step (R_{p1}), and so the observed impedance may indicate a slow CO_2 diffusion, which may be due to slow chemical surface adsorption/desorption and/or slow surface-diffusion processes for CO_2 reduction on the surface of $PrBaMn_2O_{5+\delta}$ at lower temperature. Although fast oxygen ion mobility would be expected due to a large concentration of ordered oxide ion vacancies in $PrBaMn_2O_{5+\delta}$, it shows lower surface activity for CO_2 reduction at lower temperature. However, fairly good performances were still achieved at temperatures higher than 800 °C and its surface activity for CO_2 may be improved if other catalytic additives are effectively employed. Due to improved surface activity, various metal catalyst additives are now under study, and the results will be reported in the future. Fig. 7 shows SEM micrographs of the cathode of the $PrBaMn_2O_{5+\delta}$|LDC|$La_{0.9}Sr_{0.1}Ga_{0.8}Mg_{0.2}O_3$ (LSGM)|La(Sr)Fe(Co)O_3 cell before and after CO_2 electrolysis. There appears to be some limited coking on the top surface that might be explained by Boudouard reaction at high temperature with CO_2/CO mixture or slow response of $PrBaMn_2O_{5+\delta}$ for the chemical surface adsorption/desorption of CO_2 molecules;

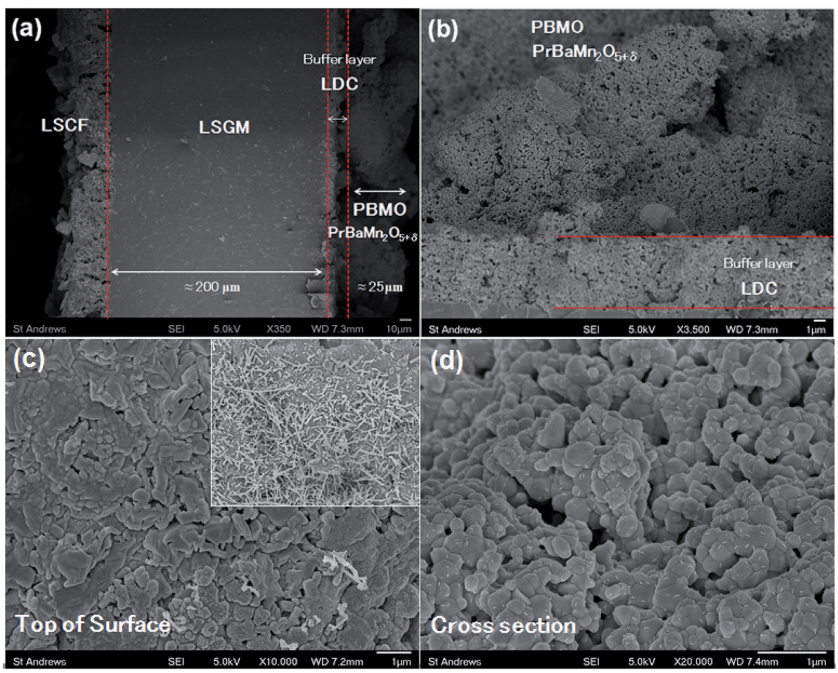

Fig. 7 SEM images of a $PrBaMn_2O_{5+\delta}$|LDC|$La_{0.9}Sr_{0.1}Ga_{0.8}Mg_{0.2}O_3$ (LSGM)|La(Sr)Fe(Co)O_3 cell after electrochemical tests, (a) cross section of the cell and (b) cathode parts include $PrBaMn_2O_{5+\delta}$|LDC, (c) the top of the surface, and (d) high magnification of the cathode.

however, there were no serious surface morphology changes. It was therefore concluded that A-site ordered layered perovskite, $PrBaMn_2O_{5+\delta}$, could be used as a potential cathode in solid oxide electrolysis with excellent redox tolerance.

4. Conclusion

In summary, $PrBaMn_2O_{5+\delta}$ was successfully prepared as a single phase cathode material from a disordered O3 perovskite phase after reduction treatment. The reduction to obtain layered $PrBaMn_2O_{5+\delta}$ can be performed *in situ* during SOEC/SOFC testing to limit processing steps. An *in situ* high temperature X-ray diffraction study confirmed the phase changes under reducing and oxidising conditions, showing that the A-site ordered layered perovskite can be formed from disordered cubic phase under reducing conditions at 800 °C with reversible phase change between $PrBaMn_2O_{5+\delta}$ (O5) and $PrBaMn_2O_{6-\delta}$ (O6) during redox cycles. The superior redox ability of $PrBaMn_2O_{5+\delta}$ (O5) was also observed by thermo-gravimetric methods, showing a reversible weight change during redox cycling corresponding to a change in oxygen stoichiometry of $\delta = 1$.

Moreover, the reduction of CO_2 *via* elevated-temperature (750–850 °C) electrolysis using an SOEC with LSGM as the electrolyte was studied using a $PrBaMn_2O_{5+\delta}$ (O5) cathode. High current density (0.845 A cm^{-2}) was obtained at 850 °C and electrolysis potential of 1.55 V for a cell using the $PrBaMn_2O_{5+\delta}$|LDC|$La_{0.9}Sr_{0.1}Ga_{0.8}Mg_{0.2}O_3$ (LSGM)|La(Sr)Fe(Co)O_3. As a result, this study revealed that $PrBaMn_2O_{5+\delta}$ (O5) is a potential cathode material for SOECs.

Acknowledgements

We thank EPSRC (EP/I022570/1, EP/K015540/1, EP/I038950/1) and the Royal Society (Wolfson Research Merit award) for support.

References

1 J. L. Bernal-Agustín and R. Dufo-López, *Int. J. Hydrogen Energy*, 2008, **33**, 6401.
2 J. O. M. Bockris and T. N. Veziroglu, *Int. J. Hydrogen Energy*, 2007, **32**, 1605.
3 S. H. Jensen, P. H. Larsen and M. Mogensen, *Int. J. Hydrogen Energy*, 2007, **32**, 3253.
4 W. Doenitz, R. Schmidberger, E. Steinheil and R. Streicher, *Int. J. Hydrogen Energy*, 1980, **5**, 55.
5 A. O. Isenberg, *Solid State Ionics*, 1981, **3–4**, 431.
6 E. H. Seymour, L. Murray and R. Fernandes, *Int. J. Hydrogen Energy*, 2008, **33**, 3015.
7 L. Schlapbach, *Nature*, 2009, **460**, 809.
8 L. Wang and R. T. Yang, *Energy Environ. Sci.*, 2008, **1**, 268.
9 B. Sakintuna, F. Lamari-Darkrim and M. Hirscher, *Int. J. Hydrogen Energy*, 2007, **32**, 1121.
10 S. D. Ebbesen and M. Mogensen, *J. Power Sources*, 2009, **193**, 349.
11 N. Q. Minh and M. B. Mogensen, *Electrochem. Soc. Interface*, 2013, **22**, 55.
12 C. Graves, S. D. Ebbesen and M. Mogensen, *Solid State Ionics*, 2011, **192**, 398.
13 K. Xie, Y. Zhang, G. Meng and J. T. S. Irvine, *J. Mater. Chem.*, 2011, **21**, 195.

14 C. Graves, S. D. Ebbesen, S. H. Jensen, S. B. Simonsen and M. B. Mogensen, *Nat. Mater.*, 2015, **14**, 239.
15 D. M. Bierschenk, J. R. Wilson and S. A. Barnett, *Energy Environ. Sci.*, 2011, **4**, 944.
16 E. P. Murray, T. Tsai and S. A. Barnett, *Nature*, 1999, **400**, 649.
17 P. Huang, A. Horky and A. Petric, *J. Am. Ceram. Soc.*, 1999, **82**, 2402.
18 B. C. H. Steele, I. Kelly, H. Middleton and R. Rudkin, *Solid State Ionics*, 1988, **28–30**, 1547.
19 S. McIntosh and R. J. Gorte, *Chem. Rev.*, 2004, **104**, 4845.
20 X. L. Yue and J. T. S. Irvine, *J. Electrochem. Soc.*, 2012, **159**, F442.
21 S. Wang, H. Tsuruta, M. Asanuma and T. Ishihara, *Adv. Energy Mater.*, 2015, **5**, 1401003.
22 Y. Li, J. Zhou, D. Dong, Y. Wang, J. Z. Jiang, H. Xiang and K. Xie, *Phys. Chem. Chem. Phys.*, 2012, **14**, 15547.
23 X. Yue and J. T. S. Irvine, *Electrochem. Solid-State Lett.*, 2012, **15**, B31.
24 X. L. Yue and J. T. S. Irvine, *Solid State Ionics*, 2012, **225**, 131.
25 F. Bidrawn, G. Kim, G. Corre, J. T. S. Irvine, J. M. Vohs and R. J. Gorte, *Electrochem. Solid-State Lett.*, 2008, **11**, B167.
26 S. Sengodan, S. Choi, A. Jun, T. H. Shin, Y.-W. Ju, H. Y. Jeong, J. Shin, J. T. S. Irvine and G. Kim, *Nat. Mater.*, 2015, **14**, 205.
27 M. T. Anderson, J. T. Vaughey and K. R. Poeppelmeier, *Chem. Mater.*, 1993, **5**, 151.
28 S. McIntosh and R. J. Gorte, *Chem. Rev.*, 2004, **104**, 4845.
29 S. B. Adler, *J. Electrochem. Soc.*, 2002, **149**, E166.
30 S. McIntosh, J. Vohs and R. Gorte, *J. Electrochem. Soc.*, 2003, **150**, A1305.